Chinese Journal of Polymer Science Vol. 32, No. 1, (2014), 9–20

Chinese Journal of Polymer Science
© Chinese Chemical Society
Institute of Chemistry, CAS
Springer-Verlag Berlin Heidelberg 2014

Size Distribution and Anisotropy of the Minor Phase Droplets in Polypropylene/Ethylene-Octene Copolymer Blends: Effects of Shear and Component Miscibility*

Cheng-zhen Geng[a], Yan-ling Zhu[a], Guang-hui Yang[a], Qiang Fu[a**], Chao-liang Zhang[b], Ke Wang[a] and Tian-nan Zhou[a]

[a] *College of Polymer Science and Engineering, State Key Laboratory of Polymer Materials Engineering, Sichuan University, Chengdu 610065, China*

[b] *State Key Laboratory of Oral Diseases, West China Hospital of Stomatology, Sichuan University, Chengdu 610065, China*

Abstract In this work, polypropylene (PP)/octene-ethylene copolymer (POE) blends were injection-molded using the so-called dynamic packing injection technique, which imposed oscillatory shear on the gradually cooling melt during the packing solidification stage. In this way, the effect of shear on the size distribution and anisotropy of the minor phase droplets could be investigated. Besides, by using two kinds of POE with different octene contents, the effect of component miscibility was also studied. The results show that the droplet size is mainly determined by composition and miscibility, and droplet anisotropy is mainly determined by droplet size and shear. Most importantly, under the same processing condition, droplet anisotropy increases with droplet size, and there seems a linear fit between them, disregarding the miscibility factor. These results may provide guidance for preparing polymer blends with desired properties by tailoring their phase morphologies.

Keywords: Shear; Miscibility; Size distribution; Anisotropy; Phase morphology.

INTRODUCTION

Blending of polymers has received much interest as a very suitable and economic alternative for the synthesis of new monomers to generate materials with tailored properties[1–5]. Because most commercial polymers are incompatible, mechanical properties of the blends are not totally determined by those of the component polymers, they are also strongly affected by processing flow conditions and the resulting phase morphology, such as droplets size distribution and droplet anisotropy[1–5]. So the key to optimizing desired final properties is the control of the phase morphology, and good insight into the relationship between the blend morphology and processing flow/temperature field is essential[1–12].

The flow-induced morphology evolution of polymer blends during processing has been a subject of abundant work both theoretically and experimentally[1, 6–10, 13–20]. In general, the development and stability of the morphology of multiphase polymer melts are complex functions of the blend composition, interfacial characteristics, rheological properties and shear conditions[2, 3, 6–10, 13–20]. During processing, the morphological evolution in polymer blends is related to mechanisms such as elongated drop disintegration, minor phase relaxation and coarsening[1–3]. Two opposite processes determine the mean size of the droplets subjected to blend

* This work was financially supported by the Special Funds for Major State Basic Research Projects of China (No. 2011CB606006).
** Corresponding author: Qiang Fu (傅强), E-mail: qiangfu@scu.edu.cn
Received September 17, 2013; Revised October 5, 2013; Accepted October 9, 2013
doi: 10.1007/s10118-014-1382-4

processing: break-up and coalescence[1, 4, 6–9, 11, 16, 21, 22]. Both processes are known to be determined by the processing conditions[1, 4, 6–11, 16, 21, 22]. Several theoretical models have been proposed to understand the morphology evolution of polymer blends during melt blending[1, 7, 17–22].

However, the situation is usually more complex in practical processing/molding. The morphology formed during blending is stable only in the particular flowing field[1–3, 10, 22, 23]. If the morphology is not directly quenched from the melt, far different morphologies may be observed in the final articles due to the coupling effect of flow and temperature field[1–3, 10, 22]. For instance, during injection molding with relatively high injection speed, a skin layer with highly oriented phase morphology (fibril) could be obtained due to elongational forces arising during fountain flow at the front and to shear flow after the front has passed. This morphology, which varies much from that in the melt after blending, could be frozen in the product in close contact with the mold. In the inner zone, however, fibril disintegration and coalescence take place due to elastic recovery and/or break-up of the fibrils, resulting in spherical droplets. In this way, a macroscopic hieratical structure is formed in the product[5, 10, 24, 25]. To obtain desired phase morphology of the blends, new processing techniques are in urgent demand to control the phase morphology not only in the blending stage but also in the molding stage.

Thanks to the fast progress of mechanical technique, a variety of new processing techniques such as shear controlled orientation injection molding (SCORIM)[26], dynamic packing injection molding (DPIM)[5, 10], vibration-assisted injection molding (VAIM)[27], gas-assisted injection molding (GAIM)[28], ultrahigh-speed shear processing[29, 30], co-extrusion technique[31, 32] and die/roller-draw[7, 33] have been developed, and various external fields such as shear[5, 26, 29, 30], extension[33] and ultrasonic[34] can also be nicely introduced into polymer processing to tailor the microstructures/properties of the materials. These techniques offer new opportunities and possibilities to investigate the microstructures (droplets size distribution and droplet anisotropy) in polymer blends during/after processing/molding. However, most work focused more on the properties of the product than on the microstructure evolutions[5, 26, 27, 29–33].

So in this work, DPIM was adopted to control the phase morphology of a model polypropylene (PP)/ethylene-octene copolymer (POE) blend. This blend was chosen because it is a typical toughening system with wide-spread applications[2, 3, 8, 11, 23, 35], and our previous work demonstrated that droplet size distribution and anisotropy had a major impact on the final properties of the product[5]. The main feature of DPIM is that the melt is forced to move repeatedly in a chamber by two pistons moving reversibly with the same frequency after it was injected into the mold[5, 10, 24, 36]. In this way, samples dominated by shear-induced microstructures were obtained and the effect of shear on phase morphologies could be studied. On the other hand, most published works on droplet anisotropy were focused on the effect of shear and droplet size, and the contribution of component miscibility to droplet anisotropy was seldom discussed because it is always accompanied by the change of droplet size[7, 8, 11]. So we also tried to differentiate the contribution of component anisotropy from that of the droplet size in this work. The phase morphologies in different directions (viewed along the shear flow or perpendicular to the flow direction) were checked to get an overall three-dimensional picture of phase morphology. The results will provide a deeper insight into the influences of shear flow and component miscibility on the phase morphologies of the final product.

EXPERIMENTAL

Materials

Isotactic polypropylene (PP) T30S, a commercial product of Dushanzi Co. Ltd, China, was adopted as basal resin. Two kinds of POE with different octene contents and roughly the same molecular weight were purchased from Dow Chemical and used as toughening elastomers. Further details on properties and designations of PP and POE are provided in Table 1.

Table 1. Properties and designations of the materials used

Mark name	Density (g/cm^3)	Octene ontent	M_n	M_w/M_n	T_m[a] (°C)	MFI[b] (g/10 min)
T30S	0.91	0%	390000	4.6	168	2.1
8450	0.902	12%	44400	2	98	4
8400	0.87	24%	43800	1.96	60	35

[a] DSC measurements were performed at a heating rate of 10 K/min.
[b] MFI of both PP and POE were tested at 200 °C (2.16 kg).

Sample Preparation

Various binary blends were prepared by varying the POE content in *i*PP matrix, with the POE contents of 0, 10%, 20%, 30% and 40% by weight, respectively. Melt blending a pair of polymers was conducted using a TSSJ-25 co-rotating twin-screw extruder with the barrel temperature of 200 °C and the screw speed of 110 r/min. To prepare the anisotropy samples, the blends were molded by dynamic packing injection molding (DPIM), in which oscillatory shear (10 s^{-1}) was imposed on the gradually cooled melt during the packing solidification stage. The detailed experiment procedure has been described in references[5, 24, 37]. For comparison, injection molding under static packing was also carried out by using the same processing parameters but without shear. The processing parameters are listed in Table 2.

Table 2. Processing parameters in dynamic packing injection molding

Parameters	Values
Injection pressure	90 MPa
Injection speed	80 cm^3/s
Oscillating packing pressure	4 MPa
Oscillating frequency	1.0 Hz
Holding time	*ca*. 4 min
Melt temperature	200 °C
Hold temperature	Room temperature (about 25 °C)

The samples obtained by DPIM are called dynamic samples (D), while the samples obtained by static packing injection molding are called static samples (S). The as-obtained blends are labeled according to the POE mark name, weight content of POE and molding condition. For example, 8450-10-D represents the blended sample with 10 wt% 8450 molded by DPIM.

Characterization and Testing

Polarized optical microscopy (POM)

To examine the hierarchical structure of the injection-molded bars, a Leica RM2245 microtome was used to cut a 30 μm slice from the injection-molded bars vertical or parallel to the flow direction. The sample slice was placed between two glass slices and then inspected on a Leica DMIP microscope equipped with crossed polarizers. The pictures were recorded with a Canon Power-Shot 550 digital camera.

Scanning electron microscopy (SEM)

Scanning electron microscopy (SEM) experiments were performed to investigate the rubber domain morphologies. The panorama of the rubber domain morphology was obtained by cryo-fracturing the samples both parallel and vertical to the flow direction in liquid nitrogen and then etching them in xylene at 60 °C for 40 min. The surfaces were coated with gold and inspected using an FEI Inspect F SEM instrument with an acceleration voltage of 20 kV.

The SEM images were processed and analyzed using an Image pro plus software, to elucidate the statistical size distribution of the minor phase particles. As a size parameter, we chose the droplet area independent of their anisotropy. The droplet anisotropy was characterized by two parameters, aspect ratio and deformation factor. Aspect ratio is calculated by the ratio between major axis and minor axis of ellipse equivalent to the droplet. And deformation factor (*DF*) is calculated by $DF = P^2/4\pi S$, where P is the average perimeter of the droplets, and S is the average area of the droplets. For sphere particles, $DF = 1$, increased *DF* means enlarged deformation. The

statistical size distribution, average area, aspect ratio and deformation factor were directly analyzed or calculated by the Image pro plus software.

RESULTS AND DISCUSSION

Hierarchical Structure and 3-D View of Phase Morphology

It has been extensively reported that a hierarchical structure with a highly oriented skin and a nearly isotropic core exists in injection-molded polymers[25]. To examine the shear-induced change of macroscopic structure, polarized optical microscope (POM) was used to compare the dynamic samples with the static samples, and the images are presented in Fig. 1. For the static sample, a typical skin-core structure could be observed. The thickness of the skin layer is about 0.4 mm. In contrast, the oriented layer in the dynamic sample is much thicker (about 1.9 mm), dominating the whole area. Apart from the skin and core layer, the additional thickness of the oriented layer in the dynamic sample should be the result of the repeated shear on the melt during the solidification stage. So this layer is called the shear layer. These results correlate well with our other works on the DPIM samples[5, 37]. The corresponding layer in the static samples is called the intermediate layer.

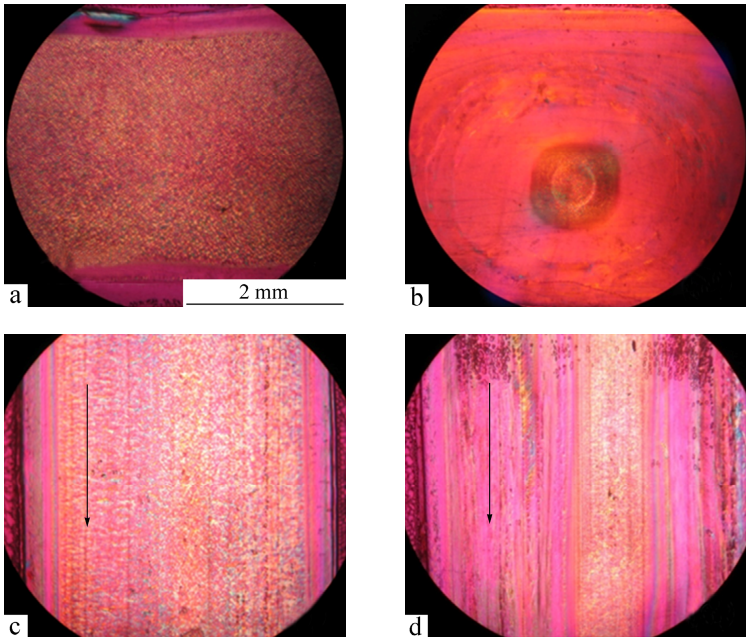


Fig. 1 Optical microscope observation of hierarchical structure of the PP/POE blends: (a) and (b) viewed along the flow direction; (c) and (d) viewed vertical to the flow direction ((a) and (c) 8400-30-S; (b) and (d) 8400-30-D. The black arrows in the figures indicate the flow direction.)

To get an overall 3-D view of the phase morphology of various samples, SEM observation was conducted both parallel and vertical to the flow direction at about 0.2 mm, 1 mm and 2.1 mm from the sample surface, representing the skin layer, intermediate/shear layer and core layer of the samples, respectively. The results for 8450-20-S and 8450-20-D are shown in Fig. 2 and Fig. 3, respectively.

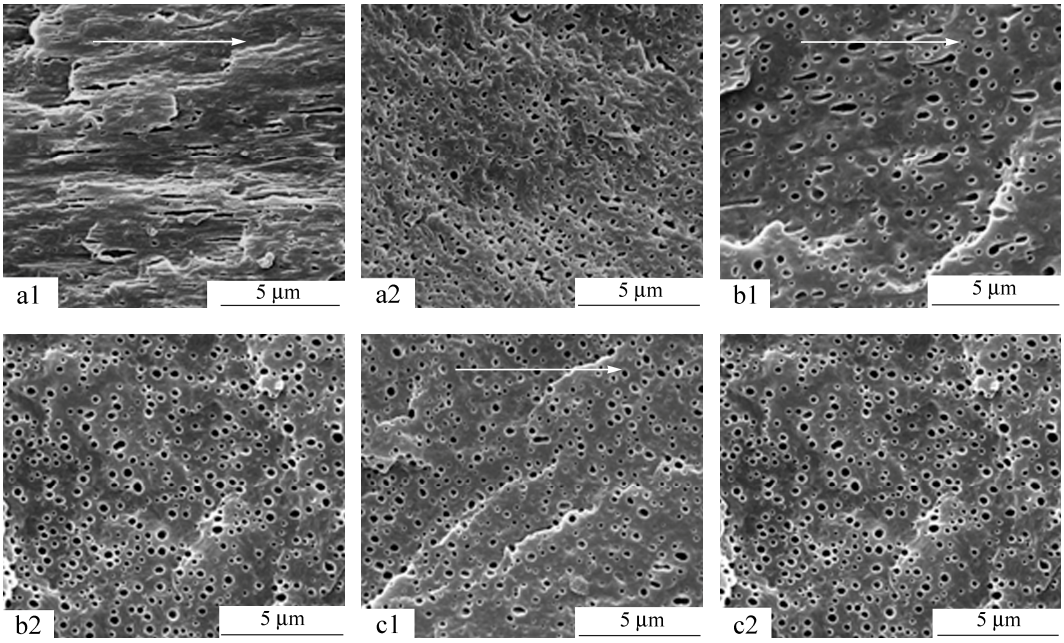


Fig. 2 SEM micrographs of phase morphology of 8450-20-S: (a) skin layer, (b) intermediate layer and (c) core layer
1 represents micrographs viewed vertical to the flow direction and 2 represents micrographs viewed along the flow direction. The white arrows in the figures indicate the flow direction.

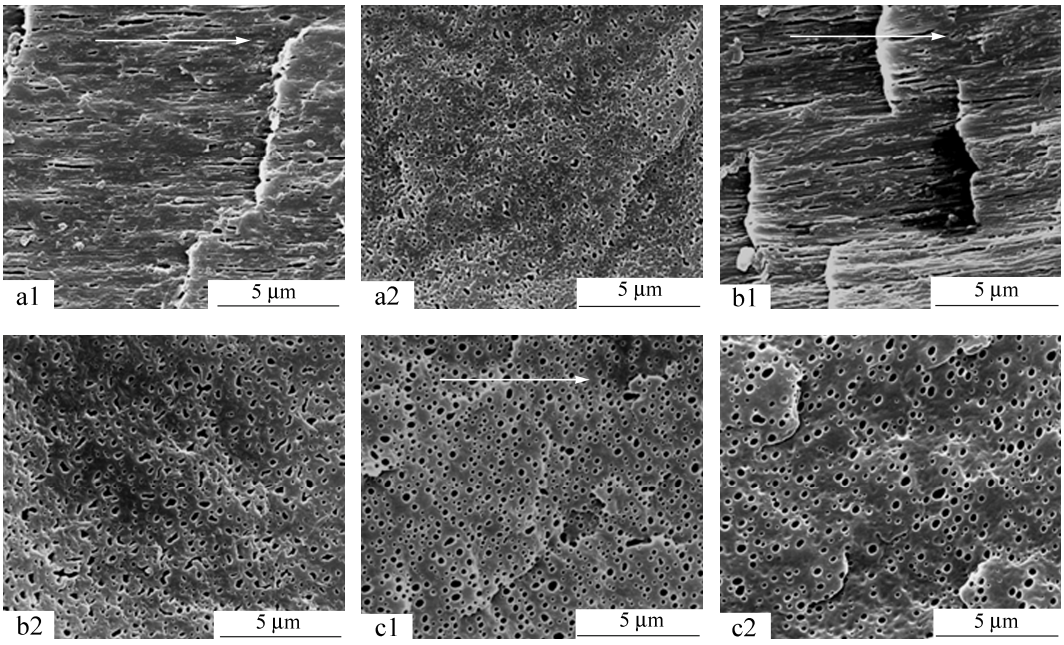


Fig. 3 SEM micrographs of phase morphology of 8450-20-D: (a) skin layer, (b) shear layer and (c) core layer
1 represents micrographs viewed vertical to the flow direction and 2 represents micrographs viewed along the flow direction. The white arrows in the figures indicate the flow direction.

As can be clearly observed, the skin layers of both static and dynamic samples show an elongated morphology along the flow direction and a rather irregular morphology vertical to the flow direction. This should

be the result of interplay between dispersed phase evolution and matrix crystallization as discussed in the Introduction part. When moving deeper to the intermediate layer of the static sample, the dispersed phase is only slightly elongated to an ellipse morphology combining the parallel and vertical view, possibly due to the combined effect of the residual stress of the fountain flow and the matrix solidification. In contrast, the shear layer of the dynamic sample presents a similar morphology to that of the skin layer, resulting from the exerted shear of DPIM on this layer. The only difference between the shear layer and the skin layer is that the domain size in the shear layer seems a little larger. This may be because of the longer time for phase separation or coalescence in this layer. Phase morphologies in the core layer of both samples are also similar, which are sphere-like domains dispersed in the matrix. To give an overall view of the hierarchical structure in the samples, a sketch of the 3-D phase morphologies in both the static and the dynamic samples is drawn, as presented in Fig. 4.

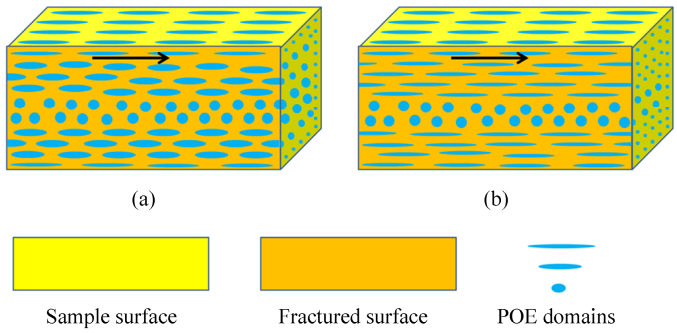


Fig. 4 A 3-D sketch showing the hierarchical structure and microstructures of (a) static samples and (b) dynamic samples
(The black arrows indicate the flow direction.)

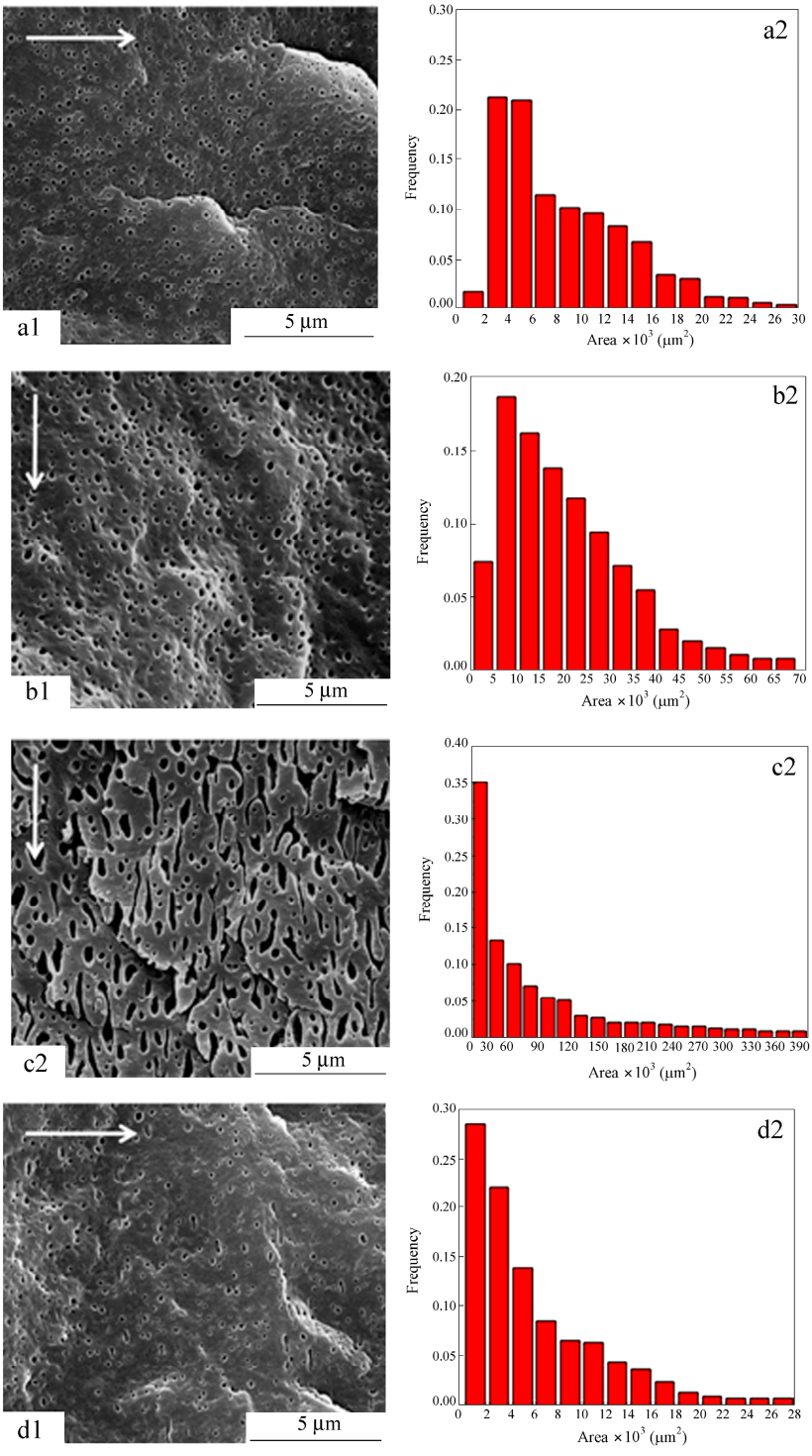
Since the main differences lie between the shear layer of the dynamic samples and the intermediate layer of the static samples, most characterizations were performed on these two corresponding layers to study the effect of shear, as will be discussed later.

Effect of POE Content, Miscibility and Shear on Size Distribution and Anisotropy of Dispersed Droplets

The reason we choose two kinds of POE with different octene contents and roughly the same molecular weight is that they show different degrees of miscibility with PP. It has been well reported that POE with higher octene content has higher miscibility with PP matrix[11, 35]. So in this way, we can investigate the effect of shear and miscibility on size distribution and anisotropy of the dispersed droplets.

Figures 5 and 6 present the SEM micrographs of the phase morphologies viewed vertical to the flow direction and the corresponding droplet size distribution of PP/8400 blends and PP/8450 blends with different POE loadings, respectively. The calculated average droplet areas of various samples are listed in Table 3.

First, the droplet size increases slightly when POE loading is increased from 10 wt% to 20 wt%, then increased significantly when POE loading is increased to 30 wt%, for both blends. As is known, during mixing, the final size of the dispersed phase results from continuous breakup and coalescence of the dispersed particles[1, 7, 9, 16]. As the concentration of the dispersed phase increases, there is an increase in coalescence, so that the particles become progressively large[12]. The difference in size increasing rate indicates that the increase in the concentration of the dispersed phase first has a better effect of raising the number of domains rather than their sizes. Only when the concentration of the dispersed phase was higher than about 20 wt%, the number of domains approached to saturation and the sizes of these domains rise distinctly due to the coalescence effect. This result is consistent with other works focusing on the droplet size in this system[7, 8, 12].


a1
5 µm
a2
Frequency
Area ×10³ (µm²)
b1
5 µm
b2
Frequency
Area ×10³ (µm²)
c2
5 µm
c2
Frequency
Area ×10³ (µm²)
d1
5 µm
d2
Frequency
Area ×10³ (µm²)

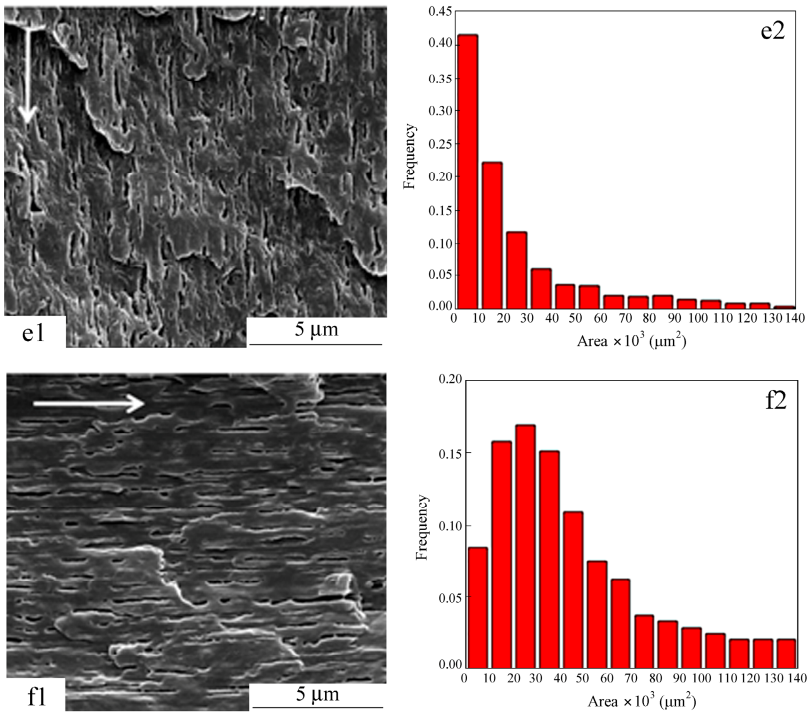
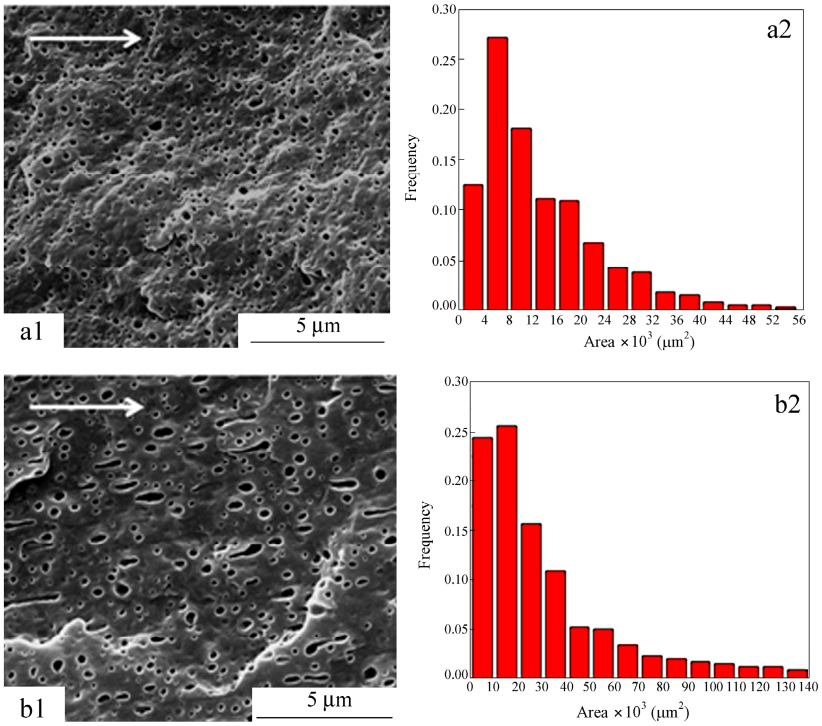


Fig. 5 SEM micrographs (1) and droplet size distribution (2) of the phase morphologies (viewed vertical to the flow direction) of (a) 8400-10-S, (b) 8400-20-S (c) 8400-30-S, (d) 8400-10-D (e) 8400-20-D, and (f) 8400-30-D The white arrows in the figures indicate the flow direction.



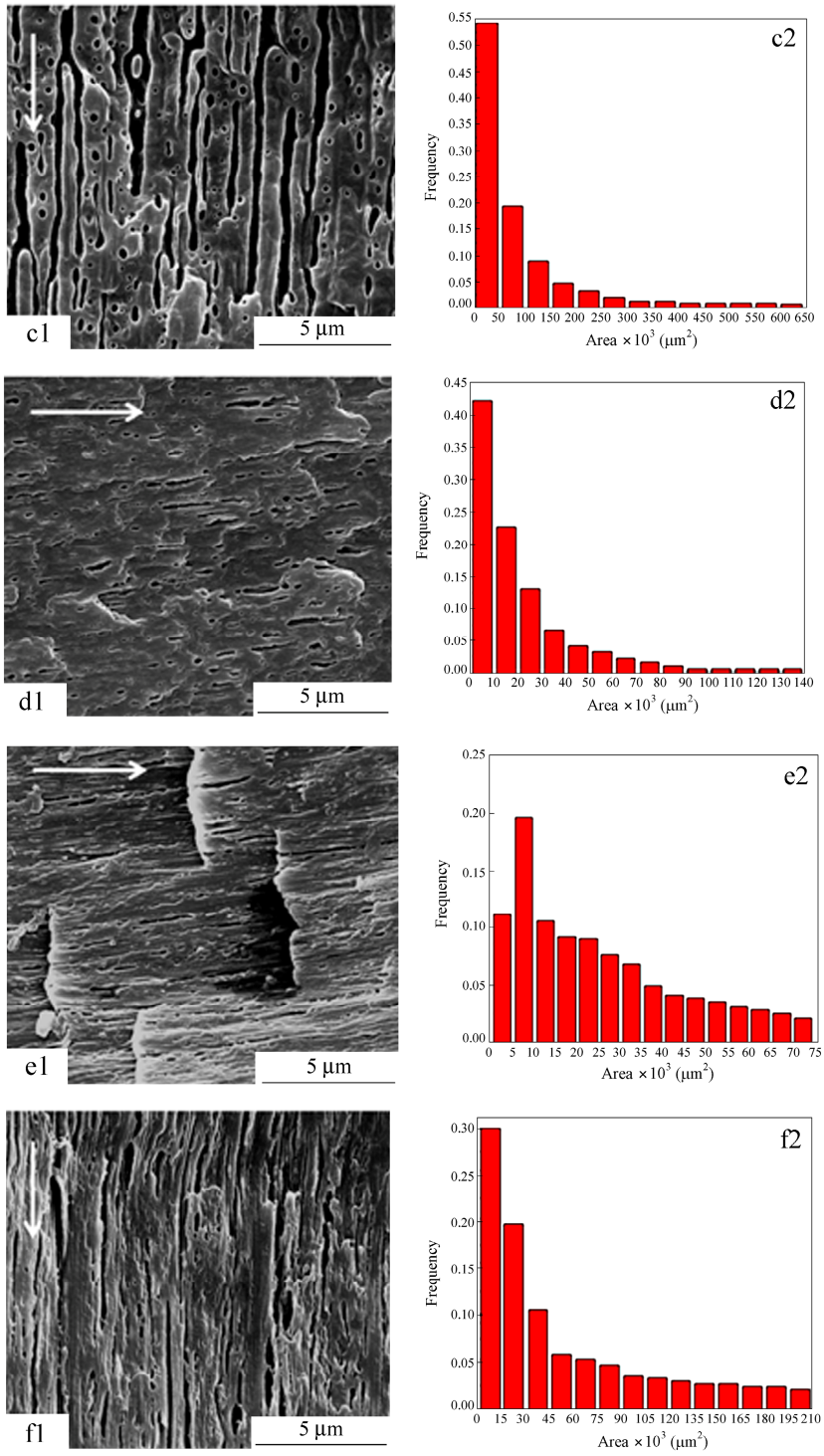


Fig. 6 SEM micrographs (1) and droplet size distribution (2) of the phase morphologies (viewed vertical to the flow direction) of (a) 8450-10-S, (b) 8450-20-S (c) 8450-30-S, (d) 8450-10-D, (e) 8450-20-D and (f) 8450-30-D The white arrows in the figures indicate the flow direction.

Table 3. Statistics of average area, aspect ratio and deformation factor of the droplets in micrographs of various samples viewed vertical to the flow direction

	Average area (μm^2)	Aspect ratio	Deformation factor
8400-10-S	0.009	1.28	1.01
8400-10-D	0.007	1.67	1.13
8400-20-S	0.021	1.51	1.09
8400-20-D	0.029	3.83	2.21
8400-30-S	0.083	2.35	1.79
8400-30-D	0.041	5.92	3.17
8450-10-S	0.014	1.39	1.04
8450-10-D	0.024	3.10	1.86
8450-20-S	0.031	1.72	1.23
8450-20-D	0.033	5.13	2.83
8450-30-S	0.096	2.68	1.92
8450-30-D	0.058	7.51	3.88

Secondly and more importantly, component miscibility also shows a dominating effect on the domain size. 8400 which has higher miscibility with PP shows smaller domain size in all the blends for both parallel and vertical view, which is consistent with many other works[5, 11, 35]. This should be the result of the difference in interfacial tension[5, 11, 35]. It has been reported in many works that polyethylene-based copolymers with higher co-monomer content has lower interfacial tension with PP in most cases[11, 35]. This should result in smaller domain size in its blends with PP.

Besides, shear also seems to have an influence on the droplet size. The direct evidence lies in the average domain size difference between 8400-10-S and 8400-10-D, both of which show a sphere morphology. The rubber domains in 8400-10-D are a little smaller than those in 8400-10-S. If this difference is acceptable, it may indicate that shear has an effect of lowering the size of droplets. However, at higher POE loadings, this phenomenon could not be concluded because the POE droplets are highly deformed for the dynamic samples.

Effect of Shear, Droplet Size and Component Miscibility on Anisotropy of Dispersed Droplets

The calculated aspect ratio and deformation factor of various samples are also listed in Table 3 for parallel view. It could be clearly seen that both shear and droplet size has a major effect on the droplet anisotropy in both PP/8400 and PP/8450 blends. At low POE contents (10 wt%), the rubber domains are rather small and very difficult to be deformed (as will be discussed later), but when the content is increased to 20 wt% or more, the morphology for the dynamic samples is changed to a highly deformed fibrillar-like structure. In contrast, their static counterpart still shows a sphere (for PP/8400) or slightly deformed ellipse morphology (for PP/8450) at the POE loading of 20 wt%. Deformation in the static samples is significantly enhanced at high POE loadings (30 wt%), but their anisotropy is still much lower than that of the dynamic counterpart, as suggested by the aspect ratio and deformation factor values listed in Table 3. When the POE content is increased to 40 wt%, all the blends show a complicated co-continuous morphology and statistics of the droplet sizes is impossible. This is out of the scope of this article and the results are not shown here.

The possible effect of component miscibility on droplet anisotropy is rather complicated because it is always accompanied by the difference in droplet size. To differentiate the effect of domain size on anisotropy from that of component miscibility, a figure presenting the anisotropy along the flow direction as a function of droplet average area is drawn, as shown in Fig. 7. Interestingly, there seems a linear fit between the droplet average area and the droplet anisotropy (both aspect ratio and deformation factor), for both the static and the dynamic samples. Higher droplet size will definitely result in higher possibility to deform. The higher slope of the linear fit for the dynamic samples could be well understood and has been discussed earlier. More importantly, both the case of PP/8400 and that of PP/8450 lie on the same linear fit when using the same processing technique. This strongly suggests that droplet anisotropy is mainly determined by droplet size and shear, disregarding the component miscibility. The miscibility could only directly determine the droplet size. This phenomenon is reported for the first time to the best of our knowledge.

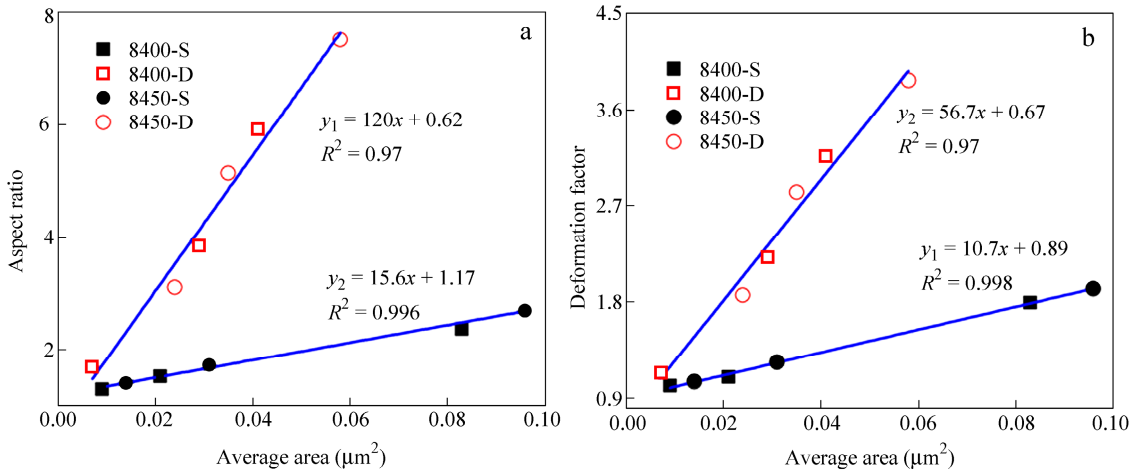


Fig. 7 Relationship between droplet anisotropy and the corresponding average droplet area: (a) aspect ratio versus droplet area and (b) deformation factor versus droplet area
The points are experimental values, and the lines are linear fitted lines of the corresponding points. The linear fitted functions are also shown in the figures

According to the pioneering work by Taylor[35, 38], the deformation of a spherical droplet under flow is closely related to two dimensionless parameters, namely the viscosity ratio ($p = \eta_d/\eta_m$, where η_d and η_m are the viscosity of the dispersed phase and the matrix phase, respectively) and capillary number ($C_a = R\eta_m \gamma/\sigma$, where R is the initial radius of droplet, γ is the shear rate, σ is the interfacial tension). Lower P and higher C_a are beneficial to the droplet deformation. This theory could correlate well with our experimental results of the linear fit between droplet size and droplet anisotropy. However, it seem controversial to our experimental results that miscibility/interfacial tension does not directly contribute to the droplet anisotropy. In other words, our results indicate that droplets with different degrees of interfacial tension should roughly deform to the same degree if they are in the same size. This deviation between the theory and our experimental results may be due to the more complicated flow of polymer melts than the Newton fluid studied by Taylor. To give a more precise description of the phase morphology of polymer blends, a new or improved theory should be developed considering the interplay between break-up and coalescence, minor phase relaxation, as well as the visco-elastic nature of polymer melts.

CONCLUSIONS

The final phase morphology of PP/POE blends is strongly related to the component miscibility and the exerted shear during the solidification stage. In particular, component miscibility has a major effect on the droplet size, and shows no direct impact on droplet anisotropy. Droplet size determines its anisotropy at the same shear condition, disregarding the component miscibility, and high shear could strongly improve the droplet anisotropy even at relatively small droplet sizes. These results may provide guidance for tailoring the phase morphologies of polymer blends and thus preparing blends with desired properties.

REFERENCES

1 Barlow, J.W. and Paul, D.R., Polym. Eng. Sci., 1981, 21(15): 985
2 Massud, D. and Abdolmajid, A., Chinese J. Polym. Sci., 2013, 31(4): 660
3 Wu, Y., Liang, X.Y., Chen, R.F., Shangguan, Y. and Zheng, Q., Chinese J. Polym. Sci., 2012, 30(3): 470
4 Li, Z. Tan, D., Ren, Q., Fu, Q., Xu, Y.F. and Tao, Y.F., Chinese J. Polym. Sci., 2013, 31(2): 363
5 Geng, C., Su, J., Han, S., Wang, K. and Fu, Q., Polymer, 2013, 54(13): 3392

6 Mei, Y., Huang, Y., He, Y. and Yang, Q., J. Appl. Polym. Sci., 2011, 124(6): 4838
7 Zuev, V.V., Steinhoff, B., Bronnikov, S., Kothe, H. and Alig, I., Polymer, 2012, 53(3): 755
8 Zhu, L., Xu, X. and Sheng, J., J. Polym. Res., 2011, 18(6): 2469
9 Verena, E. and Ziegler, B.A.W., Macromolecules, 2005, 38(13): 5826
10 Na, B., Zhang, Q., Wang, Y., Du, R. and Fu, Q., Polymer, 2003, 44(19): 5737
11 Kontopoulou, M., Wang, W., Gopakumar, T.G. and Cheung, C., Polymer, 2003, 44(24): 7495
12 Zhu, L., Xu, X., Ye, N., Song, N. and Sheng, J., Polym. Compos., 2009, 31(1): 105
13 Deyrail, R.F. and Cassagnau, P., Polymer, 2002, 43(11): 3311
14 Nino, G.O., Rheol. Acta, 1997, 36(4): 406
15 Mario, P.M. and Jan, M., Macromolecules, 1997, 30(18): 5470
16 Uttandaraman and Sundararajs, C.W.M., Macromolecules, 1995, 28: 2647
17 Elmendorp, J.J., Polym. Eng. Sci., 1986, 26(6): 418
18 Kamal, M.S., Polym. Eng. Sci., 1983, 23(11): 637
19 Lin, C.H., Polym. J., 1979, 11(3): 185
20 Taylor, G.I., Proc. R. Soc. London, 1934, 146: 501
21 Yves, A.M. and Philippe. C., Can. J. Chem. Eng., 2002, 80(6): 1017
22 Lin, D., Cheng, H., Zou, F., Ning, W. and Han, C.C., Polymer, 2012, 53(6): 1298
23 Tong, W., Huang, Y., Liu, C., Chen, X., Yang, Q. and Li, G., Colloid Polym. Sci., 2010, 288(7): 753
24 Wang, K., Chen, F. and Fu, Q., Prog. Polym. Sci., in press doi:10.1016/j.progpolymsci.2013.05.012
25 Pantani, R., Coccorullo, I., Speranza, V. and Titomanlio, G., Prog. Polym. Sci., 2005, 30(12): 1185
26 Ogbonna, G.K., Allan, P.S. and Bevis, M.J., J. Appl. Polym. Sci., 1995, 58(11): 2131
27 Kikuchi, A., Coulter, J.P. and Gomatam, R.R., J. Appl. Polym. Sci., 2006, 99(5): 2603
28 Wang, L., Wang, J.H., Yang, B., Wang, Y., Zhang, Q.P., Yang, M.B. and Feng, J.M., Colloid Polym. Sci., 2013, 291(6): 1503
29 Li, Y.J., Macromolecules, 2008, 41(14): 5339
30 Li, Y.J., Li, Z. and Hiroshi S., Macromolecules, 2008, 41(9): 3120
31 Jarus, A.H. and Baer, E., Polymer, 2002, 43(8): 2401
32 Mohit, G.Y., Taneisha, D., Eric, B., Anne H. and David A., Macromolecules, 2010, 43(9): 4230
33 Mohanraj, J., Chapleau, N., Ajji, A., Duckett, R.A. and Ward, I.M., J. Appl. Polym. Sci., 2003, 88(5): 1336
34 Guo, S., Li, Y., Chen, G. and Li, H., Polym. Int., 2003, 52(1): 68
35 Tiwari, R.R. and Paul, D.R., Polymer, 2011, 52(21): 4955
36 Liang, D., Zhou, L.J., Zhang, Q., Chen, F., Wang, K., Deng, H. and Fu, Q., Chinese J. Polym. Sci., 2012, 30(4): 603
37 Run, S., Zhang, Z., Xiang, G., Yao, G., Wang, K. and Fu, Q., J. Phys. Chem. B, 2010, 114(31): 9994
38 Grace, H.P., Chem. Eng. Commun., 1982, 14(3–6): 225